Journal of Colloid and Interface Science 513 (2018) 617–628

Contents lists available at ScienceDirect

Journal of Colloid and Interface Science

journal homepage: www.elsevier.com/locate/jcis

Regular Article

Structure and properties of epoxy-siloxane-silica nanocomposite coatings for corrosion protection

Ruben F.A.O. Torrico, Samarah V. Harb, Andressa Trentin, Mayara C. Uvida, Sandra H. Pulcinelli, Celso V. Santilli, Peter Hammer *

São Paulo State University (UNESP), Institute of Chemistry, 14800-060 Araraquara, SP, Brazil

GRAPHICAL ABSTRACT

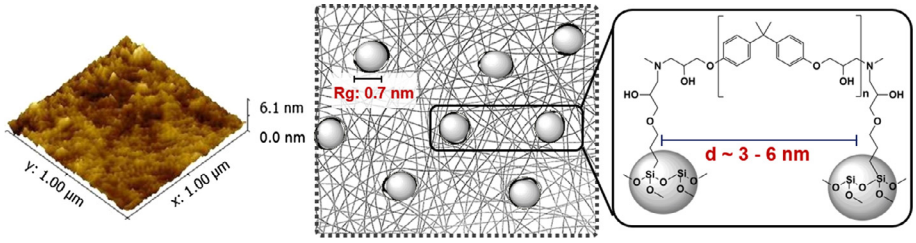

ARTICLE INFO

Article history:
Received 18 August 2017
Revised 22 November 2017
Accepted 23 November 2017
Available online 24 November 2017

Keywords:
Sol-gel process
Organic-inorganic hybrid
Structural properties
Multifunctional coatings
Corrosion protection

ABSTRACT

Hypothesis: The fraction of the silica/siloxane phase is a crucial parameter, which determines the structure and thus the properties of epoxy-siloxane-silica hybrid coatings. A careful adjustment of the colloidal precursor formulation allows tuning the nanostructure towards a highly condensed and cross-linked hybrid nanocomposite, suitable as an efficient anticorrosive coating.

Experiments: Novel epoxy-siloxane-silica hybrids have been prepared through the curing reaction of poly (bisphenol A-co-epichlorohydrin) (DGEBA) with diethyltriamine (DETA) and (3-glycidoxypropyl)methyl triethoxysilane (GPTMS), followed by hydrolytic condensation of tetraethoxysilane (TEOS) and GPTMS. At a constant proportion of the organic phase, the effects of the varying molar proportions of siloxane (GPTMS) and silica (TEOS) on the film properties have been investigated.

Findings: A detailed structural analysis suggests for intermediate TEOS to GPTMS ratios a structure of highly condensed silica-siloxane domains covalently bonded to the embedding epoxy phase. The homogeneous distribution of the quasi-spherical sub-nonmetric silica-siloxane nodes is in agreement with low surface roughness (<5 nm), observed by atomic force microscopy. This dense nanostructure results in high thermal stability (>300 °C), strong adhesion to steel substrate and excellent barrier property in saline solution, with corrosion resistance in the GΩ cm^2 range.

1. Introduction

Organic-inorganic hybrids belong to the class of nanocomposite materials, which combine two or more phases with at least one component on the nanometric length scale. Consequently, the properties of the hybrid material are not simply the sum of the contributions of each phase, but depending on the nature and type of interphase bonding, result in new materials with unique

* Corresponding author at: Instituto de Química-UNESP, Rua Prof. Degni 55, 14800-060 Araraquara, SP, Brazil.

E-mail addresses: ro1485.2011@my.bristol.ac.uk (R.F.A.O. Torrico), samarah.v.h@hotmail.com (S.V. Harb), andressinha.trentin@gmail.com (A. Trentin), mayarauvida@gmail.com (M.C. Uvida), sandrap@iq.unesp.br (S.H. Pulcinelli), santilli@iq.unesp.br (C.V. Santilli), peter@iq.unesp.br (P. Hammer).

https://doi.org/10.1016/j.jcis.2017.11.069
0021-9797/

characteristics. The nature of interphase interactions determines the type of the hybrid material. In the presence of weak interaction between the organic and the inorganic phases, such as van der Walls, ionic or hydrogen bond, the hybrid material is classified as type I, while in the case of covalent bonding the hybrid is known as type II [1]. Among the different methods to synthesize organic-inorganic hybrids, such as solution and melt blending or high-energy ball milling [2], the sol-gel process has several advantages. This is due to the mild conditions of the synthesis, homogeneous dispersion of constituents forming the colloidal solution and the possibility of combining a large number of precursors reagents at different proportions. The possibility to create a variety of new synthetic materials opens a large space for deepening the knowledge of the phenomena and mechanisms involved in the formation of hybrid networks from colloidal solutions, and this in turn allows designing and optimizing the structural properties for specific applications. Consequently, the conjugation of ceramic and polymeric phases results in multifunctional materials with interesting optical, thermal, mechanical and barrier properties, allowing a wealth of applications such as drug delivery systems, optoelectronic devices, catalysts, photochromic devices, transparent insulating films, anticorrosive coating systems, among others [1]. Concerning the latter appliance, one of the main industrial challenges is the reduction of reposition costs resulting from the corrosion of metallic components by development of economical, efficient and environmentally compliant corrosion protection methods.

The degradation of metallic materials can be either caused by mechanical wear and fatigue or by chemical processes such as dissolution, leaching and corrosion. Among these mechanisms, the corrosion process is the most common cause of failure and deterioration of metallic components. Some of the traditionally applied methods that prevent or at least delay this natural aging process involve hazardous substances as those present in the hexavalent chromium-conversion process, which forms a protective layer of insoluble trivalent chromium species. However, recent legislations impose increasing limitation on the use of toxic hexavalent chromium, still widely applied in the aeronautic industry [3,4]. Hence, the development of new efficient, low-cost methodologies to replace the use of hexavalent chromium-conversion for corrosion protection is the goal of many present research activities.

One methodology that complies with these standards is the sol-gel synthesis of organic-inorganic hybrid coatings [5]. The first attempts to synthetize this kind of material have been reported by Messadeq et al. [6] and others, such as the work of Guglielmi et al. [5]. Using a class I hybrid based on ZrO_2–PMMA (polymethyl methacrylate) they were able to increase the corrosion resistance of stainless steel by a factor of 30 [6]. Nonetheless, the weak interaction between the organic and inorganic parts caused delamination and subsequent film failure. Although there are numerous studies applying type II hybrids as anticorrosive coating [7], only few research groups succeeded to develop high performance hybrid barrier layers, which combine elevated corrosion resistance with long-term protection in aggressive environments. In these terms, very promising results were achieved for silica based hybrid coatings [8–11] and those containing corrosions inhibitors, such as cerium species [12,13]. The excellent barrier performance of these coatings have been associated with a nanostructure formed by a dense network of ramified silica-siloxane cross-link nodes covalently linked by short PMMA chains segments [10]. Despite of this progress, PMMA-siloxane-silica coatings suffer from their relatively poor thermal and mechanical properties, due to their relatively higher proportion of the PMMA phase of 70–80%.

It is known that cured epoxy polymers possess enhanced thermal and mechanical stability due to their cross-linked polymer structure provided by curing agents (hardeners). Hence the use of thermoset polymers for the synthesis of organic-inorganic nanocomposites is a promising alternative for the development of multifunctional hybrid materials, including applications such as protective coatings. In view of the innovative potential of epoxy-siloxane-silica hybrids the research activities have been considerably intensified. Matejka et al. have underlined the importance of synthesis conditions on the final structure of epoxy-siloxane-silica hybrid network [14], and a later study has demonstrated the importance of using functionalized inorganic precursor to achieve dense networks [15]. Furthermore, Nazir et al. have demonstrated that the addition of silica precursor in form of tetraethoxysilane (TEOS) and the coupling agent aminopropyltriethyoxysilane (APTES) into the epoxy matrix resulted in an increase of its thermal and mechanical stability, however anticorrosive properties of the material were not evaluated [16]. Brusciotti et al. synthetized epoxy-siloxane-silica hybrid coatings on the AZ31 Mg alloy based on different functionalized silanes linking to the epoxy phase, which has been cured using an amine hardener (diethyltriamine - DETA). The coatings with a thickness of 8–14 μm yielded a corrosion resistance of several GΩ cm^2 and durability of up to one month in pH-neutral 0.3% NaCl solution [17]. More recently, Zahed et al. achieved active corrosion inhibition for their epoxy-siloxane coatings prepared using APTES as coupling agent and a reversible tetrasulfide reagent. The 50–350 μm thick coatings, deposited on AA2024-T3 Al alloy, presented an impedance modulus in the GΩ cm^2 range during several months of immersion in 3.5% NaCl solution [18]. The cited studies [17,18] are based on the hybridization of the epoxy matrix using organosilanes, however the presence of silica, provided from an inorganic precursor, might play a crucial role for the hybrid structure and consequently its properties.

In the present study we report on a detailed structural characterization of epoxy-siloxane-silica hybrids prepared by a systematic variation the precursors proportion of silica (TEOS) and organosilane (3-glycidoxypropyl)methyltriethoxysilane (GPTMS) as coupling agent, keeping the proportion of cured epoxy to silica or organosilane constant. The fine-tuning of the proportion of colloidal precursors allows to obtain a nanocomposites structure that provides coatings with excellent thermal, mechanical anticorrosive performance, thus making them a promising alternative to conventional protective systems.

2. Materials and methods

2.1. Synthesis

All reagents were purchased from Sigma-Aldrich and used without further purification, including poly(bisphenol A-coepichlorohydrin), glycidyl end-capped (DGEBA) with an equivalent weight of 377 g/mol, diethyltriamine (DETA), (3-glycidoxypropyl)methyltriethoxysilane (GPTMS), tetraethoxysilane (TEOS), tetrahydrofuran (THF). A1020 carbon steel (dimensions of 25 mm × 25 mm × 4 mm) was used as metallic substrate, having a nominal composition (wt%) of C = 0.08–0.13%, Mn = 0.3–0.6%, P_{max} = 0.04% and S_{max} = 0.05%, with the balance consisting of Fe.

The epoxy-siloxane-silica nanocomposites were synthetized in two stages using the sol-gel route. In the first reaction step the organic component was prepared by reacting DGEBA, GPTMS and DETA in THF under stirring and reflux for 4 h at 70 °C and additional 25 min at 25 °C. The epoxy groups of DGEBA and GPTMS react with the amine groups of DETA to form a highly cross-liked network. Thereafter, TEOS, ethanol and acidified water (pH 1, using nitric acid) were added into the reflux system and the solution was stirred for an additional 1 h at 25 °C to allow the hydrolysis and condensation reactions of TEOS and GPTMS. The sol-gel reactions

produces a colloidal solution of siloxane-silica nanoparticles, which size and shape are strongly dependent on the TEOS and GPTMS proportion and other synthesis conditions such as pH, temperature and solvent proportion (ethanol/H_2O).

Two series of coatings were prepared to investigate the influence of the formulation and concentration of the silica and siloxane phase on the properties of the hybrid matrix. The first set of samples was synthetized by variation of TEOS/GPTMS molar ratio, keeping the GPTMS/DGEBA proportion constant, while in the second set the GPTMS/TEOS molar ratio was varied at a constant TEOS/DGEBA proportion. The molar composition of both series of epoxy-siloxane-silica samples (T-series and G-series) is listed in Table 1. DETA was added in a proportion that resulted in one oxirane group for every hydrogen atom of the amine groups. The structural representation of the epoxy-siloxane-silica hybrid is shown in Fig. S1-a of the Supporting Material File, together with a representative image of the final hybrid coating on carbon steel substrate (see Fig. S1-b in the Supporting Material File).

Prior to deposition, the carbon steel substrates were wet grounded using 100, 300, 600 and 1500 SiC abrasive papers, cleaned with isopropanol for 10 min in an ultrasound bath, and dried under dry nitrogen flow. Then, the transparent and homogenous sol-gel solution was used to deposit hybrid films by dip-coating onto 3 carbon steel substrates, using a withdraw rate of 14 cm min^{-1}, 1 min of immersion, with an interval of 10 min air-drying at 25 °C, and 3 immersions. The coated substrates and the remaining solution, placed into Teflon holders, were heat treated at 60 °C for 48 h. This curing procedure ensures the liberation of volatile species and the densification of the hybrid matrix.

2.2. Characterization techniques

To study the local bonding structure of the silica phase in the hybrid and to determine the degree of polycondensation of the inorganic phase, solid-state ^{29}Si magic-angle spinning nuclear magnetic resonance (MAS-NMR) was employed. The spectra were recorded for powder samples using a VARIAN spectrometer operating at 300 MHz and 7.05 T, with a Larmor frequency of 59.59 Hz. The spectra were obtained from the Fourier transformation of the free induction decays (FID), following a single $\pi/2$ excitation pulse and a decay time of 2 s. Chemical shifts were referenced to tetramethylsilane (TMS), used as external standards. Proton decoupling was employed during acquisition of the spectra. The polycondensation degree of the inorganic phase, extracted by the deconvolution of the ^{29}Si NMR spectra using Gaussian profiles was determined with a precision of ±1%.

X-ray photoelectron spectroscopy (XPS) was applied to determine the elemental composition of the hybrids and to investigate the chemical bonding structure by the deconvolution of the carbon (C 1s), oxygen (O 1s), nitrogen (N 1s), and silicon (Si 2p) spectra. The experiments were carried out at a pressure of less than 10^{-7} Pa using a commercial spectrometer (UNISPECS UHV). The Al Kα line was used (hν = 1486.6 eV) and the pass energy for the higher solution spectra was set to 10 eV. The inelastic background of the C 1s, O 1s, N 1s and Si 2p electron core-level spectra was subtracted using Shirley's method. The composition of the near surface region was determined with an accuracy of ±10% from the ratio of the relative peak areas corrected by Scofield's sensitivity factors of the corresponding elements [19]. The spectra were fitted using the CasaXPS software without placing constraints of multiple Voigt profiles.

Table 1
Molar proportions of the epoxy-siloxane-silica hybrid precursors.

Samples	DGEBA	GPTMS	DETA	TEOS
T0.0	8	8	3.2	0
T0.5	8	8	3.2	4
T/G1.0	8	8	3.2	8
T1.5	8	8	3.2	12
T2.0	8	8	3.2	16
T2.5	8	8	3.2	20
G0.0	8	0	1.6	8
G0.5	8	4	2.4	8
G1.5	8	12	4.0	8
G2.0	8	16	4.8	8
G2.5	8	20	5.6	8

Small angle X-ray scattering (SAXS) was employed to determine the nanostructural characteristics of the hybrids. The measurements were carried out at the synchrotron SAXS beamline of the National Synchrotron Light Laboratory (LNLS, Campinas, Brazil). The SAXS beamline is equipped with an asymmetrically cut and bent silicon (1 1 1) monochromator that yields a monochromatic (λ = 1.608 Å) and horizontally focused beam. A bidimensional detector (300 Pilatus k) was used to record the SAXS intensity, I (q), as a function of the modulus of the scattering vector q, q = (4 π/λ) sin(θ/2), θ being the scattering angle. The Guinier law was used to describe the scattering intensity produced by a dilute set of silica particles dispersed in a homogeneous polymeric matrix: $I(q) = G\ \exp(-q^2R_g^2/3)$ [20]. The pre-exponential factor G depends on the difference between the average electron density Δρ between the matrix and the scattering particles, and R_g is their gyration radius. The Porod law was applied where the scattering intensity follows the power law: $I(q) = A\ q^{-\alpha}$, where $A = 2\pi\ \Delta\rho^2\ S$ and S is the interface area between the particle and the matrix. The exponent α is related to the geometry and the sharpness of the interface of the particles, in the case α = 4 the surface of the scattering object is smooth whereas for values 1 < α < 3 it shows a fractal structure [21].

The coatings thickness was determined using a Filmetrics F3-CS optical interference system, and the coating roughness was obtained by atomic force microscopy (AFM), using an Agilent Technologies 5500 instrument with silicon cantilever in the tapping mode. Using the Gwyddion software, the RMS surface roughness of the coatings was extracted in thee different regions (1 × 1 μ m^2) from AFM images.

The electrochemical characterization of the carbon steel coated samples was carried out in 3.5% NaCl saline solution by electrochemical impedance spectroscopy (EIS), using a Gamry Potentiostat Reference 600. The electrochemical cell consists of coated substrate acting as the working electrode, exposing an area of 1 cm^2 to the electrolyte, an Ag|AgCl|KClsat electrode connected to the solution through a Luggin capillary was used as reference electrode and a platinum mesh as the counter electrode. The experiments were performed at room temperature (25 °C) in a Faraday cage with 10 points per decade and a 10 mV_{RMS} sinusoidal potential was applied, in a frequency range between 50 mHz and 10 kHz. The measurements were carried out until an accentuated drop of the impedance modulus occurred, indicating the failure of the coating. Before each EIS test the open circuit potential (OCP) was measured for 5–10 min. All electrochemical measurements were performed in duplicate or triplicate.

The thermal stability of epoxy-siloxane-silica hybrids has been evaluated by thermogravimetric analysis (TGA), using a TA instrument SDT Q600. The following conditions were used: nitrogen with a continuous flux of 70 mL min^{-1}, 7 mg of sample, alumina crucible, temperature range from 25 to 800 °C, and heating rate of 10 °C min^{-1}.

Microscratch tests were performed in a Nanovea PB1000 mechanical tester located at University of São Paulo (NAPMA, USP, São Carlos, Brazil). A spherical-conical diamond tip with 200 μm radius was used at an increasing load (1–10 N) on a 3 mm track at a speed of 9 N/min. The tracks were analyzed by both

optical microscopy, coupled to the mechanical tester, and scanning electron microscopy (SEM), using a FEI Inspect F50 microscope. All scratch measurements have been performed in triplicate to determine the average critical load for coating failure.

3. Results and discussion

3.1. Structural analysis

^{29}Si nuclear magnetic resonance has been applied to analyze the local bonding environment of the silicon atoms and to determine the connectivity of the inorganic network. Fig. 1 shows for samples of the T- and G-series two groups of resonances, denoted Q^j and T^j, which are related to the bonding structure of the polycondensation products of TEOS and GPTMS, respectively. The index j gives the number of Si—O—Si bridging oxygen bonds for a central Si atom, with maximum value of 4 for orthosilicates and 3 for organically modified silicates, the latter presenting one not hydrolysable Si-C bond. The peak intensities, which are proportional to the abundance of T^j and Q^j species, were extracted from spectra by a peak fitting procedure using Gaussian functions. It is clear from Fig. 1 that the Q^4 and T^3 resonance peaks, located at −108 ppm and −62 ppm, respectively, have the highest intensities, revealing the predominance of tetra- substituted TEOS and a tri-substituted GPTMS structures in the silica network.

The degree of connectivity of the inorganic phase, known as poly-condensation degree (C_d), has been determined using the following equation: $C_d = ((T^1 + 2\,T^2 + 3\,T^3)/3 + (Q^1 + 2Q^2 + 3Q^3 + 4Q^4)/4)\,100$, where T^j and Q^j are the relative peak intensities for the different local structures. The obtained C_d values for selected samples are presented in Table 2. For the T-series, the C_d values increased slightly with higher addition of TEOS, reaching 88% for the T2.0 sample, while for the G-series a very high connectivity of about 95% was obtained for the G1.5 hybrid. This is about 10% higher than the best values previously reported for hybrids based on siloxane-silica embedded in a methyl methacrylate (PMMA) matrix [9,10]. In fact, the increase in GPTMS amount led to a strong enhancement of the T^3 structures, and it seems to favor also the formation of Q^4 species yielding a highly ramified siloxane-silica structure in the hybrid.

The quantitative XPS analysis confirmed that the elemental composition of epoxy-siloxane-silica coatings corresponded, within the experimental error, to the nominal concentrations calculated for silicon, carbon, oxygen and nitrogen (see Table S1 in the Supporting Material File). The good agreement between the XPS and nominal values, obtained considering the complete hydrolysis and condensation of the GPTMS and TEOS alkoxy groups, supports the ^{29}Si NMR findings of a highly polycondensed inorganic phase with elevated connectivity. For such a condensed structure the variation of the silicon content in the range of 2.7–7.5 at.% resulted in a atomic fraction of the inorganic phase in the hybrids between 10.2 (G0.0) and 22.5 at.% (T2.5), respectively.

The local bonding structure of the formed hybrid network was assessed by the deconvolution of Si 2p, C 1s, O 1s and N 1s spectra. Fig. 2 compares for both series of samples the intensity ratio of the fitted XPS Si 2p spectral components corresponding to SiO_2 at 103.3 eV and C-SiO_x at 102.5 eV, related to the polycondensation product of TEOS and GPTMS, respectively. It can be observed that for the T-series the SiO_2 to C-SiO_x intensity ratio increases, while for the G-series this proportion decreases, according to the nominal TEOS to GPTMS molar ratios, being equal to 1 for the T/G1.0 sample. Additionally, representative C 1s, O 1s and N 1s spectra of the T/G1.0 sample, presented in Fig. S2 of the Supporting Material File, confirmed the formation of a chemical bonding structure that corresponds to the structural characteristics of the epoxy-siloxane-silica hybrid (see Fig. S1-a in the Supporting Material File).

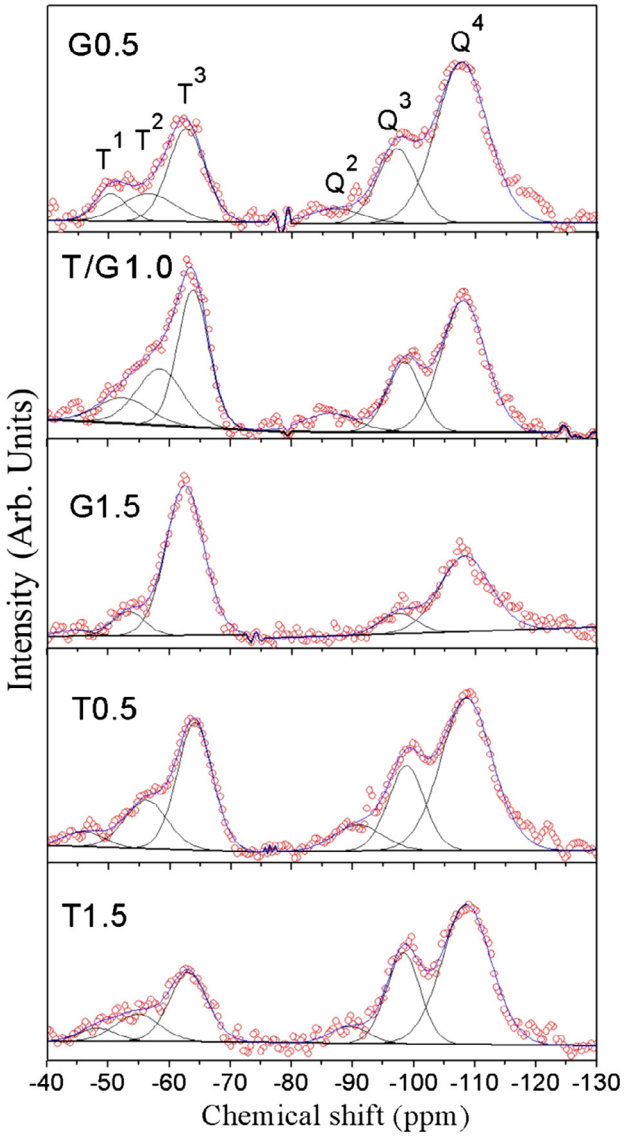

Fig. 1. Deconvoluted ^{29}Si NMR spectra of epoxy-siloxane-silica hybrids.

Small angle X-ray scattering (SAXS) has been applied to access the nanostructural features of the inorganic phase, acting as disperse scatters of higher electronic density embedded in the polymeric matrix of lower electronic density. The log-log plots of the scattering intensities recorded for hybrids of the G- and T-series show for the majority of samples three main features (Figs. 3a and b): (i) a linear decay for low q values, corresponding to the Porod regime; (ii) a Gaussian decay in the mid q-range, characteristic to the Guinier region; and (iii) in the case of the T0.0 T0.5, T/G1.0 and T1.5 hybrid a broad correlation peak superimposed to the Guinier region. This feature is related to interferences of scattered X-rays caused by the concentrated set of inorganic nano-objects, while the Guinier region is characteristic of a diluted set of scatters.

Similar scattering patterns, already observed for other silica-polymer hybrids [22,23], have been attributed either to a hierarchical organization of silica nano-domains or to bimodal family of particles. However the hierarchic aggregation model is not consistent with the existence of large and dense scatters suggested by the

Table 2
Structural properties of epoxy-siloxane-silica hybrids: polycondensation degree, C_d, (^{29}Si NMR); Porod coefficient, α, gyration radius, R_g, and correlation distance, d, (SAXS).

Samples	C_d (%)[a]	α	R_g (nm)	d (nm)
T0.0	–	–	–	3.7
T0.5	85.0	3.8	–	4.2
T/G1.0	84.0	3.2	0.7[b]	5.2[b]
T1.5	87.0	3.9	0.7[b]	5.4[b]
T2.0	88.0	3.5	0.8	–
T2.5	–	3.4	0.8	–
G0.0	–	3.8	–	–
G0.5	88.0	–	0.7	–
G1.5	94.5	4.0	0.6	–
G2.0	–	4.0	0.4	–
G2.5	–	4.0	0.3	–

[a] Error: ±0.5%.
[b] Approximate values due to the overlap of correlation peak and Guinier region.

experimental value of the Porod exponent $3.2 < \alpha < 4$ (Table 2). Hence, a bimodal family of silica nanoparticles embedded in the polymer matrix can describe the nanostructure of the epoxy-siloxane-silica hybrids. In the case of the diluted system, the average size of the smaller particles can be determined, in terms of the radius of gyration, R_g, by fitting the Gaussian decay observed in the mid q-range using the Guinier model (Table 2) [20]. In the case of the concentrated set of nanoparticles the scattering curves present a correlation peak (T0.0–T1.5) and the correlation distance ($d \approx 2\pi/q_{max}$) can be extracted from the peak position q_{max} (Table 2). The form of the larger scattering objects was obtained by fitting the linear decay of the scattering intensity for $q < 0.5$ nm^{-1} using Porod's power law model [21]. Except for the sample G0.5, showing no Porod decay in the studied q range, the determined Porod exponents of G series samples were close to 4, indicating that the silica domains consist of large (>20 nm) and homogeneous objects (dense non-aggregates) with sharp and smooth interface. On the other hand, Porod exponents found for the T series were somewhat smaller than 4 ($3.2 < \alpha < 4$), indicative of scattering by the rough surface of large silica particles.

Additionally, some clear correlations between these parameters and the increasing siloxane/silica concentration of the G- and T-series can be established. For the G-series, the evolution of the scattering pattern evidences the role of GPTMS in controlling the size of primary silica particles. The addition of increasing amount of GPTMS affects significantly the average size and the modality of silica particles as evidenced by the appearance of Guinier regime and its shift to higher q-region. The power law decay over one decade observed for the hybrid prepared without GPTMS (G0.0), indicative of monomodal size distribution of very large silica particles (>30 nm), disappears for the G0.5 sample, confirming the important role of the coupling agent in preventing the growth of silica particles and consequently in enhancing the connectivity of the hybrid network. The unique features observed for the G0.5 sample, showing an extended plateau for $q < 0.1$ nm^{-1}, evidence the presence of a monomodal family of nanoparticles with average Guinier gyration radius (R_g) of 0.7 nm, as illustrated by the structural representation of this hybrid in Fig. 3c. As a consequence, this sample presents elevated nanostructural homogeneity, owing to its highly condensed monomodal and diluted set of silica nanodomains embedded in a highly cross-linked epoxy matrix. This might be responsible for the superior corrosion protection performance of the G0.5 coating, as discussed below.

In the case of the T-series the SAXS data indicate the presence of a bimodal system with a constant density of siloxane nodes (GPTMS polycondensation product) linked to the polymeric phase. The correlation peak observed for samples without and with addition of small amount of TEOS is characteristic for a concentrated set of siloxane-silica nanoparticles. The correlation distance increases with the addition of TEOS, probably due increasing size of co-condensated siloxane-silica nodes, and disappears for highest TEOS addition. In this case the Porod regime of large particles shifts towards the Guinier regime of the smaller siloxane-silica domains, thus forming a bimodal family of nanoparticles of less distinct size.

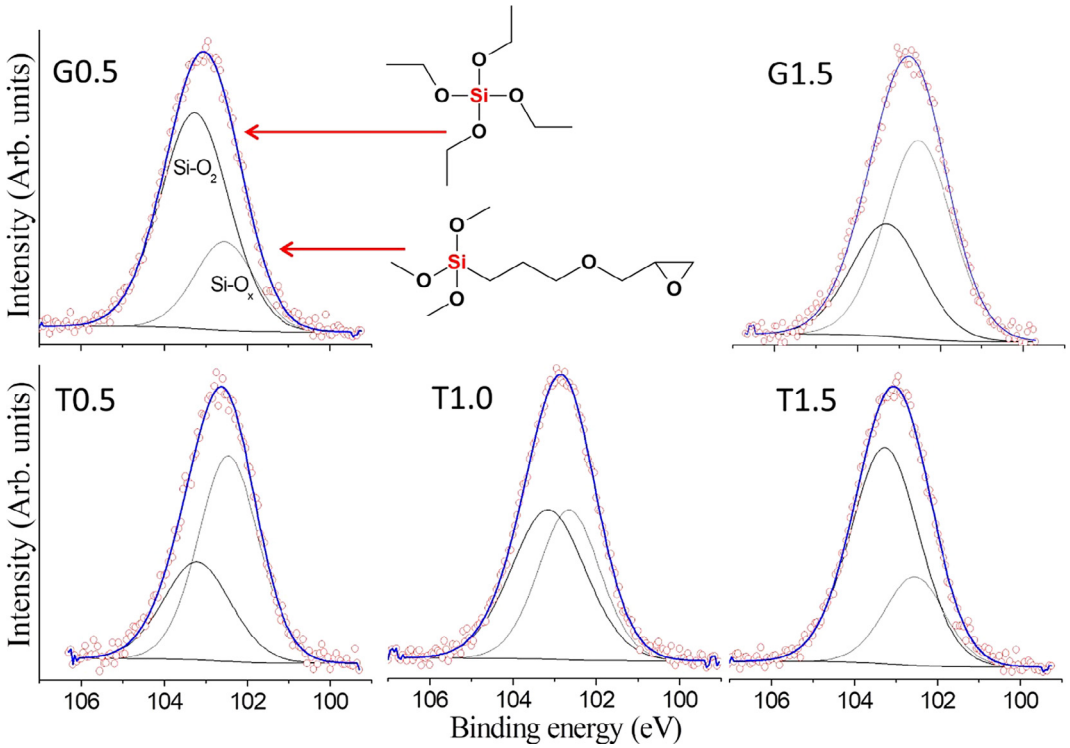

Fig. 2. Deconvoluted XPS Si 2p spectra of the epoxy-siloxane-silica hybrids.

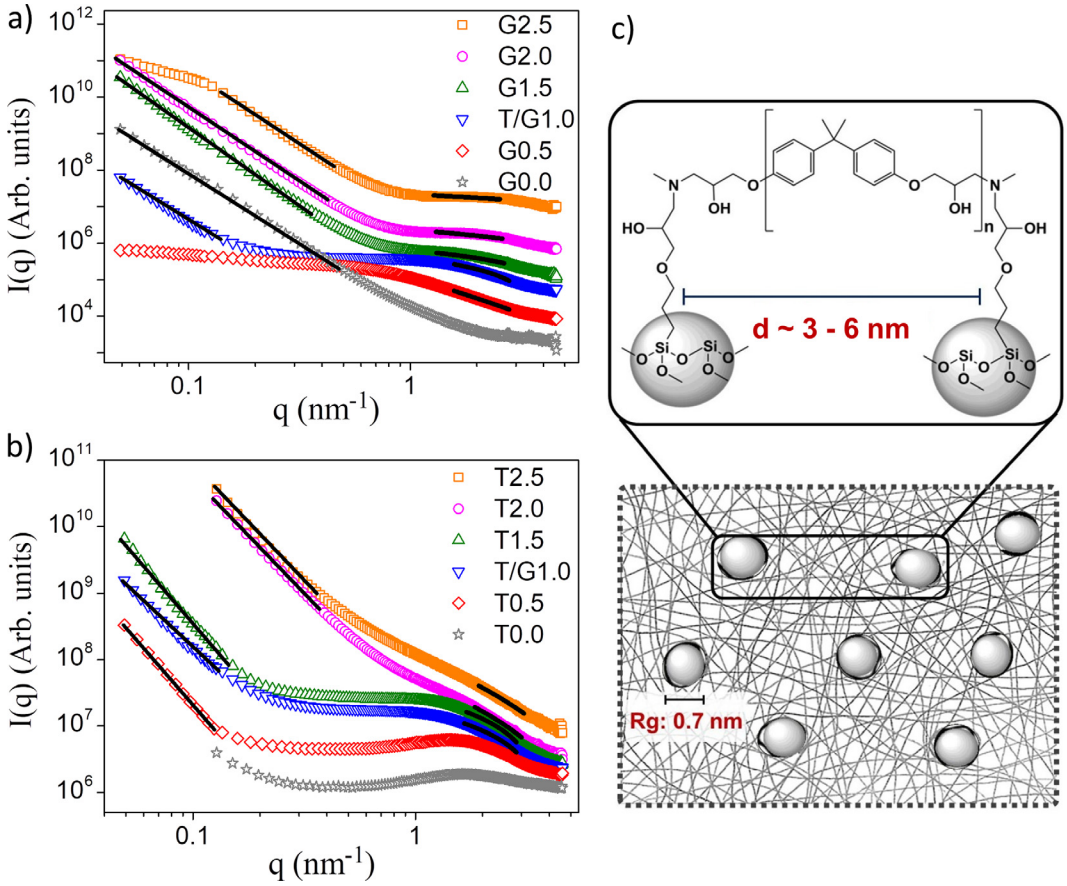

Fig. 3. SAXS curves recorded for T-series (a), and G-series (b), with black lines representing fits according to the Porod (q < 1) and Guiner (q > 1) model. (The curves were shifted for a better visualization). (c) Structural representation of the G0.5 epoxy-siloxane-silica hybrid.

In general, all these findings support and complement the NMR results indicating that for intermediate TEOS to GPTMS ratios the homogeneously distributed quasi-spherical inorganic domains consist of a highly condensed and dense siloxane-silica network covalently bonded to the epoxy matrix. As shown below, these structural features play an important role on the morphology, thermal stability, mechanical resistance, and especially on the anticorrosive performance of the coatings. A careful tuning of the nanostructure by systematic variation of the proportion of colloidal precursors results in homogeneous and dense hybrid nanocomposite suitable for efficient corrosion protection of metallic surfaces.

3.2. Coating morphology

The hybrid coatings, deposited on carbon steel, were transparent, colorless, defect free and homogeneous (Fig. S1-b), with exception for G0.0 sample that presented non-homogeneous surface due to the absence of covalent bonding between the inorganic and the organic phases. The topography images, obtained by AFM (Fig. 4), have been used to extract the RMS roughness, listed in Table 3. The results show that the films are very smooth for all samples, except T2.5, with the tendency of roughness increases for higher GPTMS to TEOS ratios. Higher TEOS proportion has a larger impact on the surface roughness than that of GPTMS, due to higher density of larger silica domains, probably associated with elevations (white spots) in the AFM images. This results are in agreement with nanostructural features derived by SAXS. As GPTMS interacts covalently with the organic phase, it is reasonable to assume that the formation of larger silica particles is suppressed in the case of hybrids of the G-series, leading to a smoother surface. This is most evident for the G0.5 film showing a very smooth surface (Fig. 4 and Table 3). On the other hand, formation of silica clusters of about 100 nm, reported for epoxy-silica hybrids, revealed microscopic phase separation for high silica concentrations, affecting the optical transparency of hybrid films [16]. Consequently, small inorganic domains produced at intermediate TEOS to GPTMS ratios (G0.5 and T1.5) yield a more homogeneous hybrid structure with enhanced interphase compatibility.

Films thickness measurements showed for all samples small values, about 1–2 μm for the G-series, and 1–7 μm for the T-series (Table 3). The larger thickness variation observed for the T-series might be related to the higher viscosity of the hybrid solution with increasing TEOS loading.

3.3. Corrosion protection efficiency

The anticorrosive efficiency of the coatings deposited on carbon steel has been tested using electrochemical impedance spectroscopy (EIS) in standard saline solution (3.5% NaCl). The coating performance was evaluated in terms of the magnitude of the impedance modulus at low frequency (5 mHz), associated with the corrosion resistance, and its long-term stability in aggressive media, referred as coating lifetime. The latter is the time span until a significant resistance drop occurs, indicating the onset of a corrosive process at the coating/metal interface. For all epoxy-siloxane-silica coatings the EIS data were recorded after 1 h of immersion in saline solution (Table 3).

The Bode plots of Figs. 5a and b show that the highest impedance modulus of up to 1 GΩ cm^2 was achieved for T1.5 and G0.5 samples, having intermediate silicon concentration (5.8 at.% and

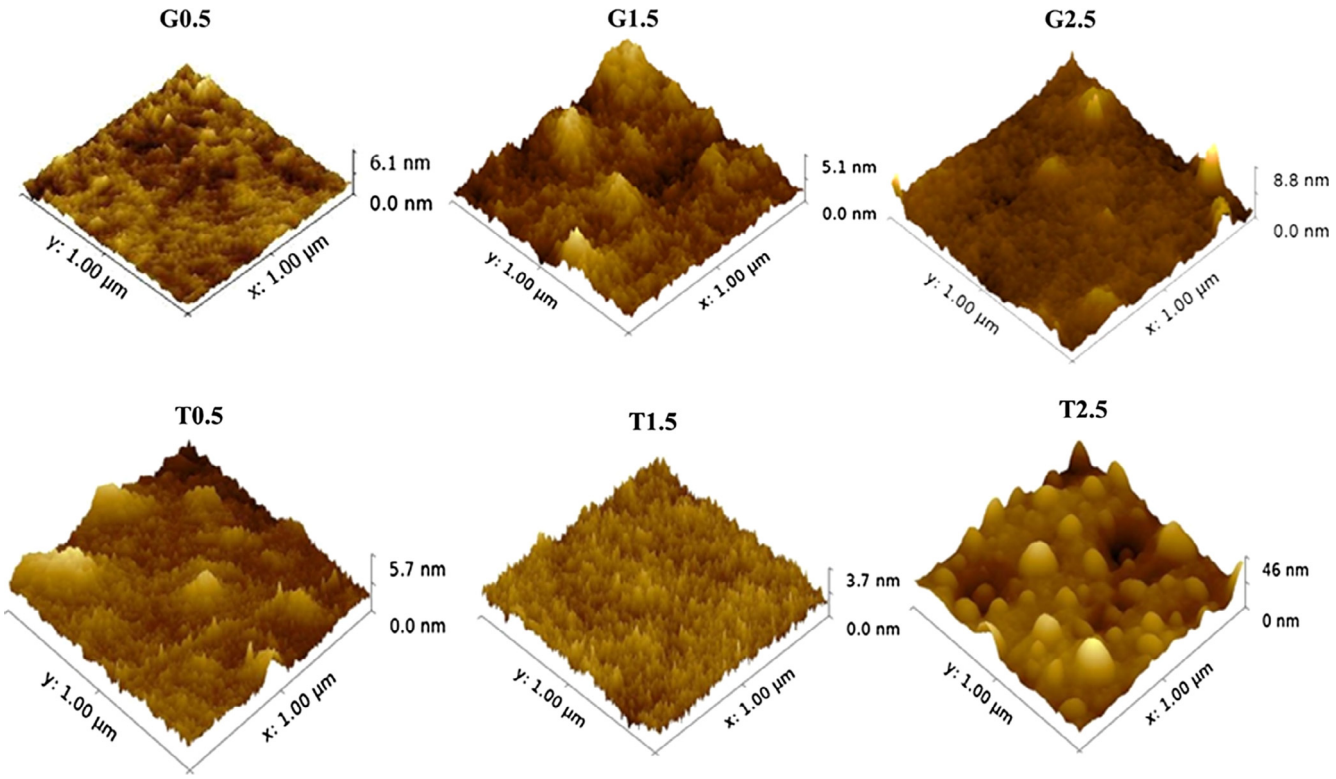

Fig. 4. 3D AFM surface topography images of epoxy-siloxane-silica coatings deposited on carbon steel.

Table 3
Properties of epoxy-siloxane-silica coatings on carbon steel: film thickness; RMS surface roughness (AFM); open circuit potential (OCP), impedance modulus at low frequency (|Z|) after 1 day immersion, and coating lifetime in 3.5% NaCl solution (EIS).

Samples	Thickness (µm)	RMS roughness (nm)	OCP[a] (V)	|Z|[a] (Ω cm^2)	Coating lifetime[b] (days)
T0.0	3.0	0.3	−0.53	3×10^6	1/1
T0.5	2.0	0.7	−0.53	7×10^6	2/1
T/G1.0	1.6	1.2	−0.48	7×10^6	5/2
T1.5	6.7	0.3	−0.08	7×10^8	42/38
T2.0	3.3	2.6	−0.54	1×10^5	1/1
T2.5	1.8	5.0	0.01	2×10^7	4/2
G0.5	1.8	0.6	−0.02	3×10^8	55/20
G1.5	1.8	0.8	−0.50	2×10^5	1/1
G2.0	1.6	1.0	−0.56	4×10^5	1/1
G2.5	1.8	1.4	−0.51	1×10^5	2/2

[a] Average values (duplicate/triplicate).
[b] Lifetime values obtained for two coatings (duplicate).

4.8 at.%) and a C/Si ratio of 11.3 and 14.1, respectively (see Table S1 in the Supporting Material File). Compared to the EIS profile of bare carbon steel, these epoxy-siloxane-silica coatings show more then four orders of magnitude higher corrosion resistance. The broad semi-circle (Fig. 5c) and capacitive phase angle dependence (Fig. 5d), which extends over about 4 decades, as well as the most anodic open circuit potential (Table 3) are additional indicators of the high passivation character of the G0.5 and T1.5 coatings. Consequently, these coatings showed the best long-term stability of 42 (T1.5) and 55 days (G0.5) in saline medium (Table 3).

To evaluate the electrochemical processes taking place during the exposure of the coatings, an equivalent circuit (inset Fig. 5c) was used to fit the EIS curves for the best performing G0.5 and T1.5 samples. The combination of two parallel RC circuits suggest the presence of two times constants, one in high frequencies (HF) range and a second at low frequencies (LF). R_1 and CPE_1 are related to the HF resistance and constant phase element of the upper film layer suffering water uptake, while R_2 and CPE_2 are associated with coating resistance and capacitive response at low frequencies of the preserved film layer at the coating/steel interface [10]. The model parameters, listed in Table 4, show that both coatings present higher resistance values of the inner layer (R_2 > 100 MΩ c m^2) compared to that of the water uptake zone. After weeks of exposure of the G0.5 coating the resistance of the upper layer (R_1) decreased about one order of magnitude due to the electrolyte permeation, while R_2 showed only a slight reduction. In the case of T1.5 coating, a larger drop of R_1 and R_2 has been observed, which can be explained by the expansion of the water uptake layer towards the coating/steel interface, indicating a more open structure of this coating.

The corrosion resistance of epoxy-siloxane-silica coatings reported here is by far superior to widely applied chromates [24,25], prepared by the toxic hexavalent chromium-conversion process. Indeed, these hybrid coatings represent a promising alter-

native to conventional coating systems as they show an improved corrosion protection when compared to coating materials based on organic [26–28], inorganic [29] and organic-inorganic hybrids [27–31]. Although thick organic coatings usually present excellent corrosion protection, the lack of adhesion to the metallic substrates limits their durability. On the other hand, inorganic coatings are able to form covalent bonds to the metal substrate; however, residual porosity and the tendency to formation of micro-cracks tend to reduce their barrier properties. As alternative, the combination of organic and inorganic phases in form of hybrid films has brought a significant impovement in the field of protective coatings in terms of thermal stability, adhesion, corrosion resistance and durability, although a number of film formulations, reported so far, present low impedance modulus (<10 MΩ cm^2) and short life time in saline solution (<30 days) [27–29]. Consequently, the improvement of corrosion resistance up to GΩ cm^2 and about two months of durability for epoxy-siloxane-silica coatings highlight the importance of a careful adjustment of the colloidal precursors to tailor the nanocomposite properties.

Although there are some recent studies reporting on longer durability in 3.5% NaCl solution, they refer either to thicker coatings [18] or other hybrid coating systems, such as PMMA-silica hybrids, which present lower thermal stability and mechanical resistance [9,10]. The excellent barrier properties obtained for only some microns thick G0.5 and T1.5 films can be related to a optimum proportion between the organic and inorganic phase at intermediate TEOS to GPTMS ratio, which according to NMR, SAXS and AFM results leads to a uniform distribution of a diluted set of highly condensed silica nano-clusters interacting covalently with epoxy segments (Table 2), resulting in a very smooth film surface (Table 3).

In addition to the barrier properties, thermal stability and mechanical resistance was investigated to explore the applicability of the coatings in abrasive and hot environments, as discussed in the following section.

3.4. Thermal and mechanical analysis

The thermal properties of the hybrids have been studied by thermogravimetric analysis (TGA), under nitrogen flow. The TGA and DTG (derivative) curves, displayed in Fig. 6, show that in a non-oxidative environment the epoxy-siloxane-silica hybrids present four degradation events, three related to the decomposition of the organic phase and one related to the inorganic phase. The weak first event (T_a) above 200 °C is associated with the elimination of the hydroxyl groups (dehydration) [32] which leads to the formation of an unsaturated structure (Fig. 6 – inset). The principal event (T_b) at about 380 °C involves the scission of the allylic C—C

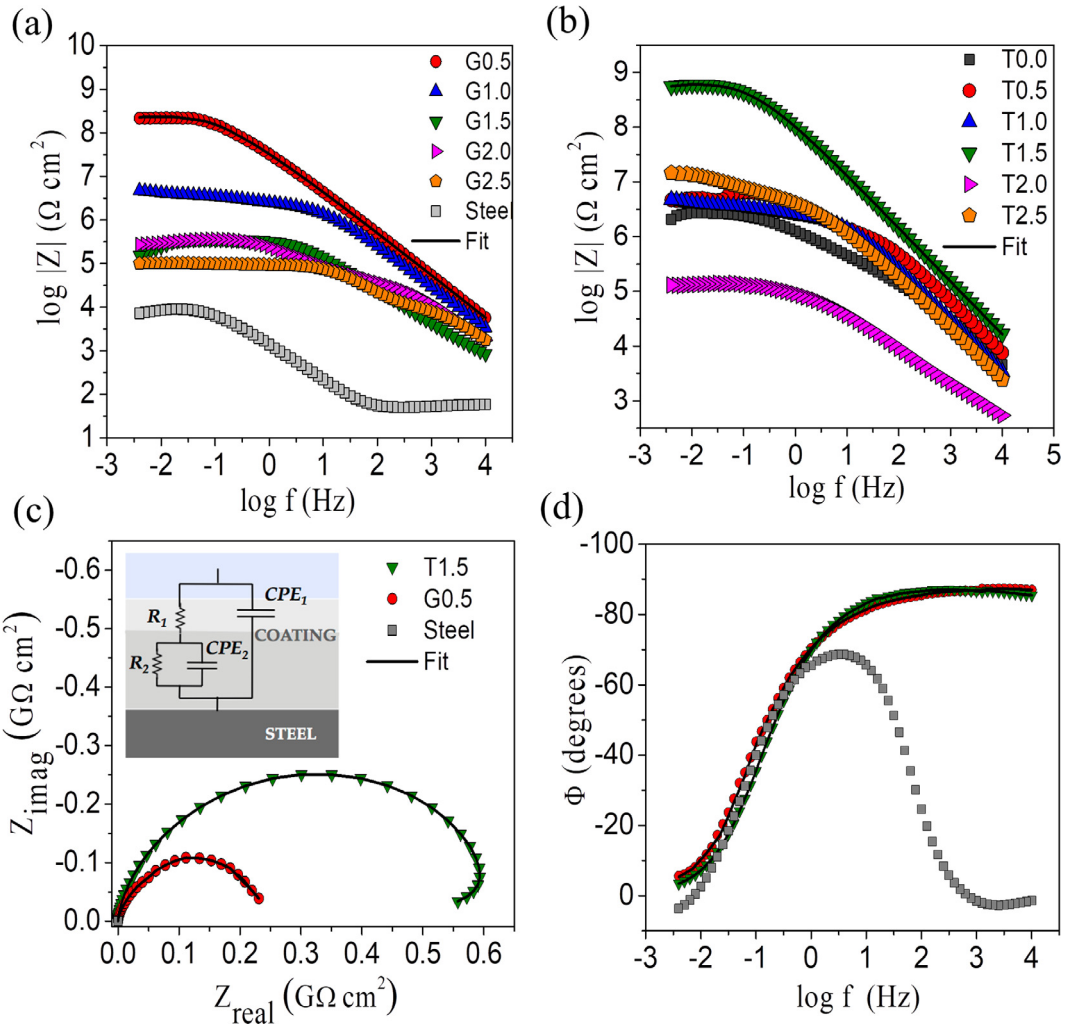

Fig. 5. Bode impedance plots recorded for epoxy-siloxane-silica coatings of (a) the G-series, including the bare steel substrate, and (b) the T-series after 1 h of immersion in 3.5% NaCl saline solution. (c) Complex plane and (d) Bode phase angle plots of best performing samples (G0.5 and T1.5). For these coatings the EIS curves were fitted according the equivalent circuit, shown in the inset of (c).

Table 4
Parameters of the electrical equivalent circuit obtained for sample G0.5 and T1.5 after 1 h exposure and 55 (G0.5), 42 (T1.5) days immersion in neutral 3.5% NaCl solution.

Sample	G0.5 (1 h)	G0.5 (55 days)	T1.5 (1 h)	T1.5 (42 days)
χ^2	5.28×10^{-4}	3.82×10^{-4}	1.92×10^{-3}	1.18×10^{-3}
R_1 (MΩ cm^2)	13.0 (6.6)	1.95 (9.6)	206.2 (6.9)	0.88 (5.6)
CPE$_1$ (nΩ^{-1} cm^{-2} s^{n-1})	1.49 (1.1)	1.56 (1.1)	1.41 (0.8)	1.92 (3.7)
n_1	0.95 (0.1)	0.95 (1.1)	0.96 (0.1)	0.95 (1.1)
R_2 (MΩ cm^2)	161.0 (0.7)	35.8 (0.7)	416.7 (3.9)	64.2 (0.4)
CPE$_2$ (nΩ^{-1} cm^{-2} s^{n-1})	2.07 (1.1)	4.21 (1.4)	1.66 (7.1)	5.65 (1.8)
n_2	0.67 (3.1)	0.60 (0.7)	0.73 (3.0)	0.75 (0.4)

Values between brackets represent the fitting errors (%).

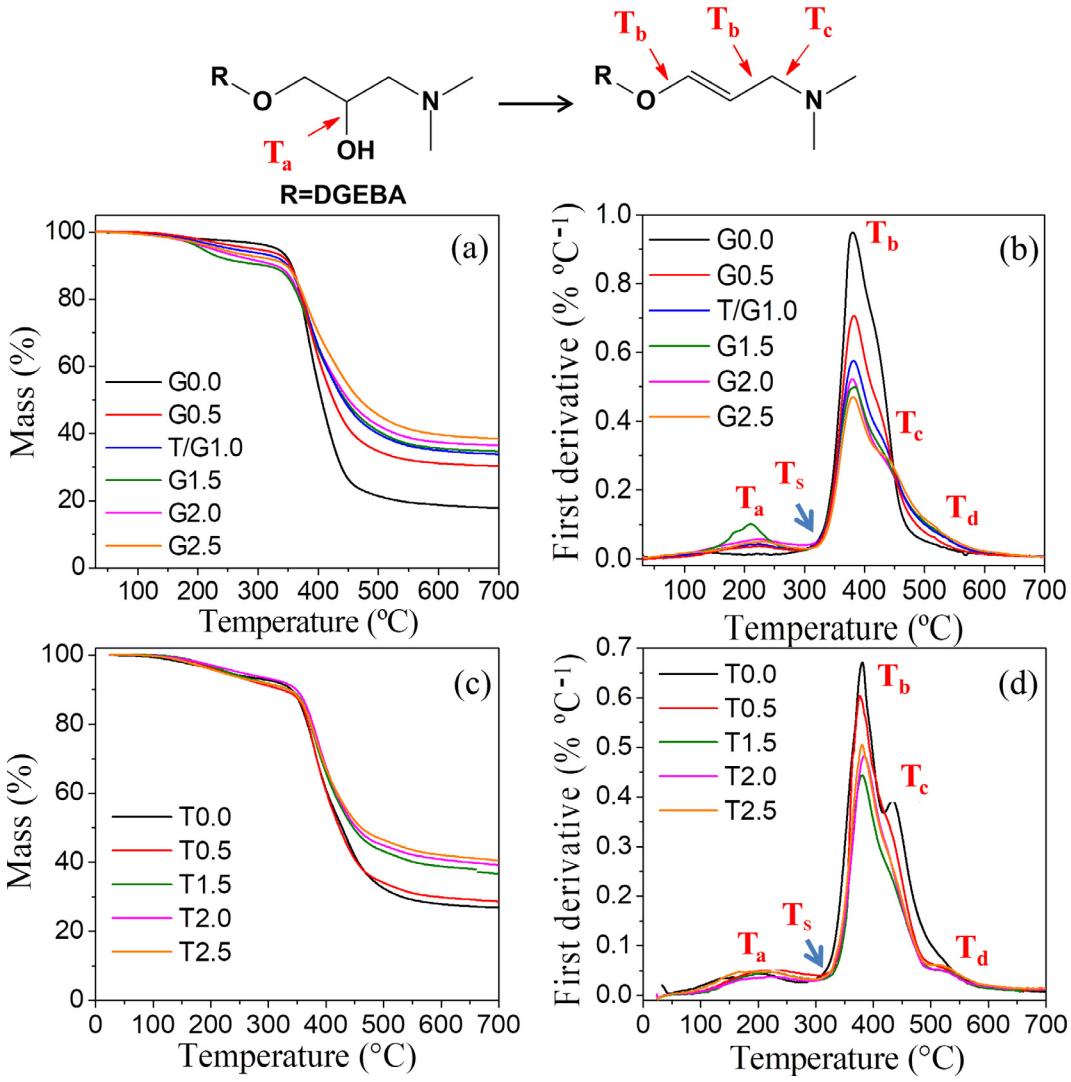

Fig. 6. TG (a) and DTG (b) curves obtained for G-series hybrid samples. TG (c) and DTG (d) curves of the T-series. Inset: decomposition events of the hybrid structure.

bonds and allylic ether C—O bonds [32,33], while the third event (T_c) at about 440 °C results from the breaking of N—C bonds (Fig. 6 – inset) [32]. The last event (T_d) at about 530 °C is related to formation of SiO_2 from partially condensed silanol ($SiO_x(OH)_y$) species [34]. The higher thermal stability of the N—C bond with respect to the C—C bond is related to its higher binding strength [35]. This is due to the dehydration reaction which favors a more stable bond as consequence of the delocalization of the double C=C bonds into the aromatic ring's vicinity [35]. The main events of the hybrid decomposition and the residue percentage at high temperature (700 °C) are summarized in Table S2 of the Supporting Material File.

The critical temperature (T_s), an important parameter that marks the thermal stability at 5% mass loss, varied between 217 °C (G1.5) and 320 °C (G0.5) and reached the highest values for samples with intermediate silica content, while the temperatures of the main degradation event (T_b) remained essentially unchanged for all samples (~385 °C). With increasing TEOS addition, the temperature of the T_c event (N—C bond breaking) gradually decreases from 440 °C (T0.0 sample) to 430 °C (T2.5 sample), while for increasing GPTMS this event increases from 430 °C (G0.0 sample) to 450 °C (G2.5 sample). Dyakonov et al. [36] have shown that the main depolymerization event in cured epoxy resins shifts towards higher temperatures when the cross-linking density

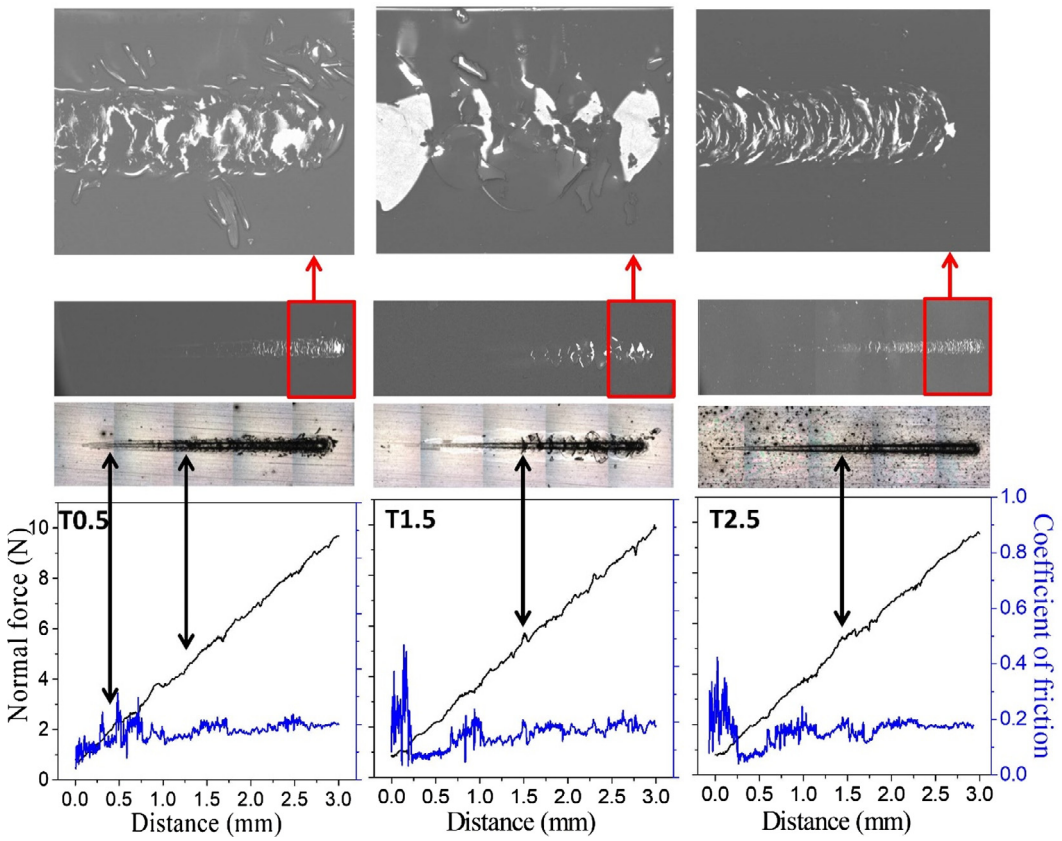

Fig. 7. Microscratch curves and scratch tracks analyzed by optical and electron microscopy for coatings of the T-series.

increases, which may explain the shift of the T_c event to higher temperature for samples prepared with increasing GPTMS and DETA addition. Although the highest T_s and T_b temperatures are similar to those reported for DETA cured DGEBA epoxy resin [32,37], a comparison with results obtained for other hybrid materials, such as PMMA-silica, shows that the thermal stability is about 100 °C higher (G0.5) [9,38], highlighting the superior thermal properties of the epoxy-siloxane-silica material. The elevated thermal stability comes from the highly cross-linked hybrid structure provided by the curing agent (DETA) and the coupling agent (GPTMS) combined with the high connectivity of the silica phase, as derived from ^{29}Si NMR data.

Micro-scratch measurements were carried out to access the mechanical properties of coatings, in terms of the coefficient of friction, mechanism of failure and surface/coating adhesion strength, which scales with the critical load of delamination (L_c). Using a diamond tip with a 200 μm radius, the scratch tests have been performed with increasing load (1–10 N) over a 3 mm long track. Fig. 7 presents the microscratch plots and the corresponding tracks, analyzed by optical and electron microscopy for coatings of the T-series. A detailed analysis of the microscopy images revealed that the coatings present different failure events, marked by black arrows in Fig. 7. The coating with small TEOS addition (T0.5) shows at a load of 2.2 N the propagation of cracking, and at higher loads (L_c = 4.6 N) the formation of spallation in form of buckling. For the sample with intermediate silica content (T1.5) presented both cracking and chipping, starting at a normal force higher than 5.7 N, while the sample T2.5 (highest Si content) presented only spallation in form of buckling at normal force higher than 5.9 N. The increase of the critical load of delamination, observed for coatings with higher silica content, can be related to their improved adhesion to the steel substrate due to increasing number of covalent bonds formed at the coating/steel interface between silanol (Si—OH) and iron hydroxide (Fe—OH) groups. It is interesting to note that this remarkable adhesion, observed for high loads, has been achieved for some micrometers thick films deposited on merely sanded carbon steel.

The friction coefficient presented similar values for all measured samples, showing small variation around 0.2 over the entire scratch track. This relatively low friction coefficient can be associated with the large fraction of polymeric phase forming the hybrid, as determined by XPS and TGA, as well as with the low coating roughness (<5 nm), observed by AFM. Although the obtained values for the critical force are well above of those found for PMMA-silica coatings reinforced by carbon nanotubes [39], a direct comparison with reported results is in this case not feasible. This is due to the fact that the friction coefficient and the critical load of delamination do not depend only on the structure and adhesion of the coating but also on a number of experimental parameters such as tip radius, loading rate, substrate material, coating thickness and internal stress, among others. Nevertheless, the exploration of the structural properties of the coating/steel interface is an important and challenging task to be tackled in future studies. This information would be of particular importance for the interpretation of electrochemical data after long-term assays of coated samples in aggressive environments.

4. Conclusions

Epoxy-siloxane-silica hybrid nanocomposites with excellent anticorrosive, thermal and mechanical properties were developed to act as protective coatings for metallic surfaces. By varying the molar ratio between the coupling agent (GPTMS) and the inorganic

precursor (TEOS) the effects of the siloxane-silica to epoxy proportion on the nanostructure, composition and morphology have been investigated and the results were correlated with thermal, mechanical and electrochemical barrier properties. In a in-depth structural investigation it was found that the best performing samples containing silicon in the lower concentration range, possess a hybrid structure that is composed of homogeneous distribution of almost spherical highly condensed siloxane-silica nano-domains covalently bonded to a cross-linked epoxy matrix, yielding homogeneous, transparent, defect free and extremely smooth coatings (R_{RMS} < 1 nm) with a thickness of less than 7 μm. The highly reticulated structure of the films resulted in a barrier layer with high corrosion resistance of up to 1 GΩ cm^2 and durability of several weeks in aggressive environment, a performance which is superior to that of most anticorrosive coatings reported so far [26–31], including the environmentally problematic chromates coatings [24,25]. Furthermore, the combination of a thermoset polymer covalently bonded to silica-siloxane phase yielded a hybrid nanocomposite with thermal stability of up to 320 °C, significantly higher than others organic-inorganic hybrids with comparable anticorrosive performance, such as the PMMA-SiO_2 system [9,10]. In addition, the hybrid coatings presented an excellent adhesion to the steel substrate due to the presence of silica phase at the coating/steel interface, providing covalent bonding with the substrate, which led to a critical load for delamination of up to 5.9 N. These results confirmed that by the careful adjustment of the proportion of TEOS and GPTMS colloidal precursors and thus of the ratio between the organic and inorganic phase, it is possible to obtain a highly packed hybrid structure yielding a thermal, mechanical and anticorrosive performance not achieved for similar epoxy-TEOS system, using APTES (amino-propyltriethoxysilane) as coupling agent [16,40]. However, besides elevated corrosion resistance, the long-term stability in aggressive media is essential for the applicability of the coatings. Thus to achieve a durability in the time scale of years a further improvement of the structural properties in feedback with the synthesis conditions is needed. Nevertheless, this approach constitutes a crucial step forward towards the development of high performance protective coatings being applicable in hot and abrasive environments.

Acknowledgements

We would like to thank the National Laboratory of Synchrotron Light Source (LNLS, Brazil) for the use of SAXS facilities. This work was supported by the Brazilian funding agencies CNPq, CAPES and FAPESP.

Appendix A. Supplementary material

Supplementary data associated with this article can be found, in the online version, at https://doi.org/10.1016/j.jcis.2017.11.069.

References

[1] C. Sanchez, P. Belleville, M. Popall, L. Nicole, Applications of advanced hybrid organic–inorganic nanomaterials: from laboratory to market, Chem. Soc. Rev. 40 (2011) 696–753.
[2] P.D. Castrillo, D. Olmos, D.R. Amador, J. González-Benito, Real dispersion of isolated fumed silica nanoparticles in highly filled PMMA prepared by high-energy ball milling, J. Colloid Interf. Sci. 15 (2007) 318–324.
[3] International Agency for Research on Cancer, IARC Monographs 100C: A Review of Human Carcinogens, Arsenic, Metals, Fibres and Dusts, IARC, Lyon, 2012.
[4] N.M. Gatto, M.A. Kelsh, D.H. Mai, M. Suh, D.M. Proctor, Occupational exposure to hexavalent chromium and cancers of the gastrointestinal tract: a meta-analysis, Cancer Epidemiol. 34 (2010) 388–399.
[5] M. Guglielmi, Sol-gel coatings on metals, J. Sol-Gel Sci. Technol. 8 (1997) 443–449.
[6] S.H. Messaddeq, S.H. Pulcinelli, C.V. Santilli, A.C. Guastaldi, Y. Messaddeq, Microstructure and corrosion resistance of inorganic-organic (ZrO_2-PMMA) hybrid coating on stainless steel, J. Non Cryst. Solids 247 (1999) 164–170.
[7] R.B. Figueira, C.J.R. Silva, E.V. Pereira, Organic-inorganic hybrid sol-gel coatings for metal corrosion protection: a review of recent progress, J. Coatings Tech. Res. 12 (2015) 1–35.
[8] S.H. Ammar, K. Ramesh, B. Vengadaesvaran, S. Ramesh, A.K. Arof, A novel coating material that uses nano-sized SiO_2 particles to intensify hydrophobicity and corrosion protection properties, Electrochim. Acta 220 (2016) 417–426.
[9] P. Hammer, F.C. dos Santos, B.M. Cerrutti, S.H. Pulcinelli, C.V. Santilli, Highly corrosion resistant siloxane-polymethyl methacrylate hybrid coatings, J. Sol-Gel Sci. Technol. 63 (2012) 266–274.
[10] F.C. dos Santos, S.V. Harb, M. Menu, V. Turq, S.H. Pulcinelli, C.V. Santilli, P. Hammer, On the structure of high performance anticorrosive PMMA-siloxane-silica hybrid coatings, RSC Adv. 5 (2015) 106754–106763.
[11] D.D.A. López, M.A.D. Crespo, A.M.T. Huerta, A.F. Vela, J.A. Adame, H.D. Rosales, Analysis of degradation process during the incorporation of ZrO_2:SiO_2 ceramic nanostructures into polyurethane coatings for the corrosion protection of carbon steel, J. Mater. Sci. 48 (2013) 1067–1084.
[12] J. Mosa, N.C.R. Navarro, M. Aparicio, Active corrosion inhibition of mild steel by environmentally-friendly Ce-doped organic-inorganic sol-gel coatings, RSC Adv. 6 (2016) 39577–39586.
[13] S.V. Harb, F.C. dos Santos, B.L. Caetano, S.H. Pulcinelli, C.V. Santilli, P. Hammer, Structural properties of cerium doped siloxane-PMMA hybrid coatings with high anticorrosive performance, RSC Adv. 5 (2015) 15414–15424.
[14] L. Matejka, K. Dusek, J. Plestil, K.G. Jaroslav, F. Lednicky, Formation and structure of the epoxy-silica hybrids, Polymer 40 (1998) 171–181.
[15] L. Prezzi, L. Mascia, Network density control in epoxy-silica hybrids by selective silane functionalization of precursors, Adv. Polym. Tech. 24 (2005) 91–102.
[16] T. Nazir, A. Afzal, M. Humaira, X. Siddiqi, Z. Ahmadb, M. Michel, Thermally and mechanically superior hybrid epoxy-silica polymer films via sol-gel method, Prog. Org. Coat. 69 (2010) 100–106.
[17] F. Brusciotti, D.V. Snihirova, H. Xue, M.F. Montemor, S.V. Lamaka, M.G.S. Ferreira, Hybrid epoxy-silane coatings for improved corrosion protection of Mg alloy, Corros. Sci. 67 (2013) 82–90.
[18] M.A. Zadeh, S. Van Der Zwaag, S.J. Garcia, Adhesion and long-term barrier restoration of intrinsic self-healing hybrid sol-gel coatings, ACS Appl. Mater. Interf. 8 (2016) 4126–4136.
[19] J.H. Scofield, Hartree-slater subshell photoionization cross-sections at 1254 and 1487 eV, J. Electron Spectrosc. 8 (1976) 129–137.
[20] G. Guinier, C. Fournet, C.B. Walker, K.L. Yudovitch, Small Angle Scattering of X-rays, Freeman, New York, 1955.
[21] B. Hammouda, A new guinier-porod model, J. Appl. Cryst. 43 (2010) 716–719.
[22] S. Zaioncz, K. Dahmouche, C.M. Paranhos, R.A.S. San Gil, B.G. Soares, Relationships between nanostructure and dynamic-mechanical properties of epoxy network containing PMMA-modified silsesquioxane, Express Polym. Lett. 3 (2009) 340–351.
[23] K. Dahmouche, L.D. Carlos, V. de Zea, Bermudez, R.A. Sá, Ferreira, C.V. Santilli, A.F. Craievich, Structural modelling of Eu^{3+}-based siloxane-poly(oxyethylene) nanohybrids, J. Mater. Chem. 11 (2011) 3249–3257.
[24] K.S. Aneja, S. Bohm, A.S. Khanna, H.L.M. Bohm, Graphene based anticorrosive coatings for Cr(VI) replacement, Nanoscale 7 (2015) 17879–17888.
[25] M.G.S. Ferreira, R.G. Duarte, M.F. Montemor, A.M.P. Simões, Silanes and rare earth salts as chromate replacers for pre-treatments on galvanised steel, Electrochim. Acta 49 (2004) 2927–2935.
[26] M. Ghaffari, M.R. Saeb, B. Ramezanzadeh, P. Taheri, Demonstration of epoxy/carbon steel interfacial delamination behavior: electrochemical impedance and X-ray spectroscopic analyses, Corros. Sci. 102 (2016) 326–337.
[27] S.A. Haddadi, M. Mahdavian, E. Karimi, Evaluation of the corrosion protection properties of an epoxy coating containing sol-gel surface modified nano-zirconia on mild steel, RSC Adv. 5 (2015) 28769–28777.
[28] M. Bozorg, A. Ramezani, Characterization and protective performance of acrylic-based nanocomposite coating reinforced with silica nanoparticles, Mater. Corros. 68 (2017) 725–730.
[29] R.T. Sakai, F.M. Di, L. da Cruz, H.G. de Melo, A.V. Benedetti, C.V. Santilli, P.H. Suegama, Electrochemical study of TEOS, TEOS/MPTS, MPTS/MMA and TEOS/MPTS/MMA films on tin coated steel in 3.5% NaCl solution, Prog. Org. Coat. 74 (2012) 288–301.
[30] M. Atik, F.P. Luna, S.H. Messaddeq, M.A. Aegerter, Ormocer (ZrO2-PMMA) films for stainless steel corrosion protection, J. Sol-Gel Sci. Technol. 8 (1997) 517–522.
[31] T.P. Chou, C. Chandrasekaran, S.J. Limmer, S. Seraji, Y. Wu, M.J. Forbess, C. Nguyen, G.Z. Cao, Organic-inorganic hybrid coatings for corrosion protection, J. Non Cryst. Solids 290 (2001) 153–162.
[32] V. Bellenger, E. Fontaine, A. Fleishmann, J. Saporito, J. Verdu, Thermogravimetric study of amine cross-linked epoxies, Polym. Degrad. Stab. 9 (1984) 195–208.
[33] D. Pugliaa, L.B. Manfredib, A. Vazquez, J.M. Kennya, Thermal degradation and fire resistance of epoxy-amine-phenolic blends, Polym. Degrad. Stab. 73 (2001) 521–527.

[34] C.J.T. Landry, B.K. Coltrain, J.A. Wesson, N. Zumbulyadis, J.L. Lippert, In situ polymerization of tetraethoxysilane in polymers: chemical nature of the interactions, Polymer 33 (1992) 1496–1506.
[35] N. Grassie, M.I. Guy, N.H. Tennent, Degradation of epoxy polymers: part 4 thermal degradation of bisphenol-A diglycidyl ether cured with ethylene diamine, Polym. Degrad. Stab. 14 (1986) 125–137.
[36] T. Dyakonov, P.J. Mann, Y. Chen, W.T.K. Stevenson, Thermal-analysis of some aromatic amine cured model epoxy-resin-systems-II: residues of degradation, Polym. Degrad. Stab. 54 (1996) 67–83.
[37] S. Grishchuk, Z. Mbhele, S. Schmitt, J. Karger-Kocsis, Structure, thermal and fracture mechanical properties of benzoxazine-modified amine-cured DGEBA epoxy resins, Polym. Lett. 5 (2011) 273–282.
[38] Y.T. Wang, T.C. Chang, Y.S. Hong, H.B. Chen, Effect of the interfacial structure on the thermal stability of poly(methyl methacrylate)-silica hybrids, Thermochim. Acta 397 (2003) 219–226.
[39] S.V. Harb, S.H. Pulcinelli, C.V. Santilli, K. Knowles, P. Hammer, A comparative study on graphene oxide and carbon nanotube reinforcement of PMMA-siloxane-silica anticorrosive coatings, ACS Appl. Mater. Interf. 8 (2016) 16339–16350.
[40] E. Bakhshandeh, A. Jannesaria, Z. Ranjbar, S. Sobhani, M.R. Saeb, Anti-corrosion hybrid coatings based on epoxy–silica nano-composites: toward relationship between the morphology and EIS data, Prog. Org. Coat. 77 (2014) 1169–1183.